Bioorganic & Medicinal Chemistry 26 (2018) 3453–3460

Contents lists available at ScienceDirect

Bioorganic & Medicinal Chemistry

journal homepage: www.elsevier.com/locate/bmc

Elucidating the inhibition of peptidoglycan biosynthesis in *Staphylococcus aureus* by albocycline, a macrolactone isolated from *Streptomyces maizeus*

Hai Liang[b], Guangfeng Zhou[a], Yunhui Ge[a], Elizabeth A. D'Ambrosio[b], Tess M. Eidem[c], Catlyn Blanchard[c], Cindy Shehatou[c], Vijay K. Chatare[a], Paul M. Dunman[c], Ann M. Valentine[a], Vincent A. Voelz[a], Catherine L. Grimes[b], Rodrigo B. Andrade[a,*]

[a] Department of Chemistry, Temple University, Philadelphia, PA 19122, United States
[b] Department of Chemistry and Biochemistry, University of Delaware, Newark, DE 19716, United States
[c] Department of Microbiology and Immunology, University of Rochester School of Medicine and Dentistry, Rochester, NY 14642, United States

ARTICLE INFO

Keywords:
Albocycline
MRSA
VRSA
Peptidoglycan biosynthesis inhibition
MurA

ABSTRACT

Antibiotic resistance is a serious threat to global public health, and methicillin-resistant *Staphylococcus aureus* (MRSA) is a poignant example. The macrolactone natural product albocycline, derived from various *Streptomyces* strains, was recently identified as a promising antibiotic candidate for the treatment of both MRSA and vancomycin-resistant *S. aureus* (VRSA), which is another clinically relevant and antibiotic resistant strain. Moreover, it was hypothesized that albocycline's antimicrobial activity was derived from the inhibition of peptidoglycan (i.e., bacterial cell wall) biosynthesis. Herein, preliminary mechanistic studies are performed to test the hypothesis that albocycline inhibits MurA, the enzyme that catalyzes the first step of peptidoglycan biosynthesis, using a combination of biological assays alongside molecular modeling and simulation studies. Computational modeling suggests albocycline exists as two conformations in solution, and computational docking of these conformations to an ensemble of simulated receptor structures correctly predicted preferential binding to *S. aureus* MurA—the enzyme that catalyzes the first step of peptidoglycan biosynthesis—over *Escherichia coli* (*E. coli*) MurA. Albocycline isolated from the producing organism (*Streptomyces maizeus*) weakly inhibited *S. aureus* MurA (IC_{50} of 480 μM) but did not inhibit *E. coli* MurA. The antimicrobial activity of albocycline against resistant *S. aureus* strains was superior to that of vancomycin, preferentially inhibiting Gram-positive organisms. Albocycline was not toxic to human HepG2 cells in MTT assays. While these studies demonstrate that albocycline is a promising lead candidate against resistant *S. aureus*, taken together they suggest that MurA is not the primary target, and further work is necessary to identify the major biological target.

1. Introduction

Methicillin-resistant *Staphylococcus aureus* (MRSA) infections represent a major challenge to public health.[1,2] Traditionally, these infections have been treated with vancomycin, the antibiotic of last resort. Unfortunately, MRSA and vancomycin-resistant *S. aureus* (VRSA) have emerged in the clinic, necessitating new therapeutic development.[3,4] Albocycline (**1**), a 14-membered macrolactone naturally produced by several *Streptomyces* strains (Fig. 1a), was first isolated by the Tanabe Seiyaku Company in 1967 and Upjohn (as ingramycin) in 1968.[5] However, the correct structure and absolute stereochemistry were not rigorously established until 1983 by X-ray crystallography.[6,7] Tanner and Somfai reported the first total synthesis of albocycline in 40 total steps (21 in the longest linear sequence) in 1987.[8] Recently, we reported a total asymmetric synthesis of (−)-albocycline in 14 total steps from commercial starting materials enabled by *N*-sulfinyl metallodienamines.[9]

In 2013, Tomoda and co-workers reported that albocycline displayed *in vitro* antimicrobial activity toward MRSA and was equipotent to vancomycin (MIC = 0.5–1.0 μg/mL).[10] Accordingly, albocycline represents a potential solution toward the treatment of resistant *S. aureus* infections. The 14-membered macrolactone of albocycline, a structural motif found in the macrolide class of antibiotics, suggests it targets the bacterial ribosome and therefore inhibits translation.[11] However, Tomoda and co-workers found that albocycline dose-dependently inhibits the biosynthesis of peptidoglycan (PG), the protective polymer surrounding bacterial cells, by blocking the incorporation of radiolabeled *N*-acetylglucosamine ([^{3}H]GlcNAc) into the PG of MRSA. Inhibition by

* Corresponding author.
E-mail address: randrade@temple.edu (R.B. Andrade).

https://doi.org/10.1016/j.bmc.2018.05.017
Received 14 February 2018; Received in revised form 2 May 2018; Accepted 12 May 2018
Available online 24 May 2018
0968-0896/

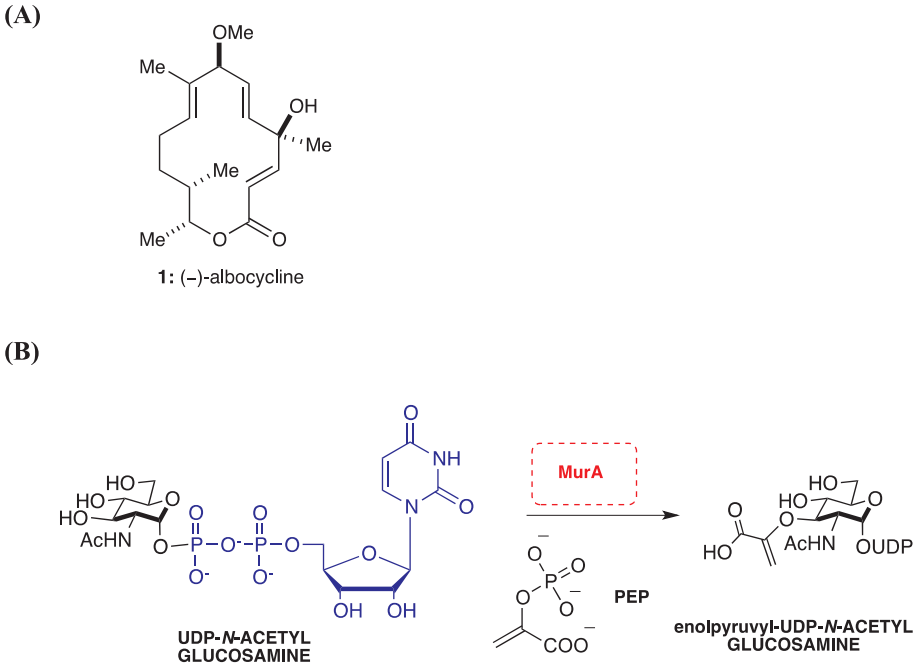

Fig. 1. First Biosynthetic step of peptidoglycan biosynthesis and proposed inhibitor: (A) Structure of (−)-albocycline (**1**), that is proposed to inhibit MurA. (B) MurA catalyzes the addition of phosphoenolpyruvate to UDP-N-Acetyl-Glucosamine to form enolypruvl-UDP-N-Acetyl-Glucosamine. UDP is urdine diphosphate shown in blue.

albocycline results in the accumulation of *N*-acetylglucosamine (UDP-GlcNAc), the first building block of bacterial PG biosynthesis.[10] We reasoned that MurA, the conserved enzyme that catalyzes the first committed step in PG biosynthesis by converting UDP-GlcNAc to enolpyruvyl-UDP-GlcNAc, was the likely target of albocycline by covalent modification (Fig. 1b).[12] This hypothesis was predicated on three key observations: (1) MurA employs a nucleophilic thiol (Cys115) in its active site critical to catalysis; (2) albocycline possesses an electrophilic α,β-unsaturated macrolactone moiety (Fig. 1b) whose site-selective hydrogenation to 2,3-dihydroalbocycline through biotransformation rendered the reduced congener inactive;[13] and, (3) validated MurA inhibitors terreic acid[14] and cnicin[15] both contain electrophilic alkenes essential to their mechanism of action (i.e., alkylation of Cys115 to effect covalent target modification).[16]

In this study, a combination of computational studies and enzyme inhibition assays were used to assess the mechanism of albocycline inhibition against MurA enzymes. Interestingly, *S. aureus* produces two homologs of MurA: MurA and MurZ, whereas *E. coli* only has MurA enzyme. Here, multiple computational methods were used to model the binding between albocycline and MurA/MurZ enzymes from *S. aureus* and MurA from *E. coli*. The computational work presented is notable for its use of several recent methodological innovations in order to address key challenges in modeling macrocycle and receptor flexibility. To accurately model the conformational preferences of albocycline, a new Bayesian inference method, BICePs,[17,18] was employed to reconcile theoretical modeling with sparse experimental NMR measurements. To model the flexibility of the MurA enzyme, ensembles of receptor structures for computational docking were generated from massively parallel molecular simulations of MurA on the Folding@home distributed computing platform. This work presents the exciting opportunity to compare predictions of these methods to the results of experiments.

MurA/MurZ enzymes from *S. aureus* and MurA from *E. coli* were purified to investigate the inhibition effect of albocycline via high-performance liquid chromatography (HPLC) based IC_{50} study. Albocycline was isolated in large quantity from cell cultures of the producing bacterium *S. maizeus*.[19] Cellular assays were employed to evaluate the antibiotic potential of albocycline against several bacterial strains and to determine its toxicity against human cells.

2. Materials and methods

2.1. Computational methods

2.1.1. Hybrid QM/REMD studies

A multi-scale QM/REMD (Quantum Mechanical/Replica Exchange Molecular Dynamics) approach was used to computationally model conformational states of albocycline in solution. First, to achieve thorough conformational sampling of all relevant conformational states, we performed REMD simulation using GROMACS[20] 4.5.4 on the Owlsnest high-performance computing cluster at Temple University. Simulations of albocycline were performed using the GAFF (General Amber Force Field) potential[21] with a Generalized Born/Surface Area (GBSA) implicit solvation model.[22] Partial charges were calculated using the AM1-BCC method.[23] REMD was performed for 4.2 μs using twelve temperature replicas ranging from 300 K to 450 K, resulting in 50.4 μs of aggregate simulation trajectory data. Swaps between neighboring temperatures were attempted every 10 ps, with acceptance ratios ranging from 83% to 92%.

To derive a set of conformational states for further analysis, we used the MSMBuilder2 software package[24] to perform hybrid *k*-medoid clustering of the trajectory data using a dihedral-angle distance metric. We found 100 conformational states to be sufficient for our analysis, as this was greater than the number of possible macrolide backbone rotamers. The free energy of each conformational state (in the GAFF potential) was calculated using the MBAR algorithm of Shirts and Chodera.[25]

While the GAFF potential is reasonably accurate for a wide range of organic molecules, accurate estimates of low-energy conformational states require a higher level theory. To obtain better estimates of conformational state energies, we optimized each of the 100 cluster generator structures using gas-phase DFT calculations (B3LYP 6–311 + g (2d,p)), an approach we previously found to work well for structure prediction of peptoid macrocycles.[26] This level of theory was previously found have a good balance of accuracy and computational efficiency.[17] We found that calculated DFT energies of each conformational state were strongly correlated with structural similarity to the two native crystal poses,[27] validating our use of the DFT energies for structural predictions (Fig. S1). Much poorer correlation is found between the REMD free energies and structural similarity (data not shown).

2.1.2. Bayesian inference of conformational populations (BICePs)

With accurate estimates of the energy of each conformational state in hand, we next used the BICePs algorithm[17,18] to refine estimates of solution-state conformational populations against experimental NMR observables. The sparse NOE and vicinal *J*-coupling constants measured for albocycline[9] give us valuable structural information, but this information reports on ensemble-average observables that cannot alone be used to refine population estimates. The purpose of the BICePs algorithm is to combine information from all-atom structural calculations and ensemble-averaged experimental observables to infer conformational populations in the most statistically unbiased way. In BICePs, the computationally predicted distribution of state populations is used as a Bayesian prior and coupled with a likelihood function to enforce the experimental restraints. The full Bayesian posterior is then sampled using Markov Chain Monte Carlo (MCMC), along with nuisance parameters to account for unknown errors. For a full description of the BICePs algorithm and its implementation, please refer to Voelz et al.[17]

2.1.2.1. Experimental restraints. Experimental distance and dihedral restraints (Table S1) are enforced using harmonic restraints, i.e. Gaussian likelihood functions with standard deviations σ_d and σ_J, respectively. Since the true error in experimental measurements is unknown, BICePs infers distributions of these values by treating them as *nuisance parameters* that are sampled along with the distribution of conformations. Similarly, the conversion of NOE intensities to distance restraints involves a proportionality constant that also has statistical uncertainty, so a scaling constant γ' on the experimental distances is included as an additional nuisance parameter. The full posterior distribution function sampled is:

$$P(X,\sigma_d,\sigma_J,\gamma') \propto \left[\frac{P(r_d(X)|\sigma_d,\gamma')}{P_{ref}(r_d(X))}\right]\left[\frac{P(r_J(X)|\sigma_J)}{P_{ref}(r_J(X))}\right]P(X)P(\sigma_d)P(\sigma_J)P(\gamma') \tag{1}$$

The bracketed terms on the right side of this expression are the likelihood functions, and the unbracketed terms are prior distributions. The likelihood functions are composed of harmonic restraints on experimental observables,

$$P(r_d(X)|\sigma_d,\gamma') = \prod_j \frac{1}{\sqrt{2\pi\sigma_d^2}}\exp(-[d_j(X)-\gamma' d_j^{exp}]^2) \tag{2}$$

$$P(r_J(X)|\sigma_J) = \prod_j \frac{1}{\sqrt{2\pi\sigma_J^2}}\exp(-[J_j(X)-J_j^{exp}]^2) \tag{3}$$

where $d_j(X)$ are the r^{-6}-averaged distances calculated for each conformational cluster X, d_j^{exp} are the experimental distance restraints, and γ' is an unknown scaling factor; $J_j(X)$ are coupling constants (calculated using Karplus relations, see Voelz et al.[17]) for each conformational cluster X, and J_j^{exp} are the experimental coupling constants. The harmonic restraints are normalized by reference potentials $P_{\mathrm{ref}}(\mathbf{r}_d(X))$ and $P_{\mathrm{ref}}(\mathbf{r}_J(X))$ to ensure that the likelihood functions have the correct statistical weight (see Voelz et al.[17] for details). The prior distribution of conformational populations, $P(X) = \exp(-f(X)/k_BT)$ comes from the computed DFT energies $f(X)$ of each conformation. Non-informative Jeffrey's priors ($P(x) \sim x^{-1}$) are used for $P(\sigma_d)$, $P(\sigma_J)$ and $P(\gamma')$.

2.1.2.2. BICePs results. MCMC sampling was performed for 10^7 steps, using energies $\lambda f(X)$, $\lambda = 0$, 0.5 and 1.0 for enhanced sampling (see Voelz et al.[17]). Results are shown in Fig. S2. A comparison of conformational populations p_i estimated using only the experimental restraints (exp), versus populations estimated using the combined computational and experimental information (QM + exp), shows how these two different kinds of information contribute to the final population estimates (Fig. S2a). Whereas many conformations are compatible with the ensemble-averaged experimental restraints, the additional use of computational information predicts a specific collection conformational states to be the most populated. About 85% of the total population comprises only ten states with the highest population estimates (Table S2). The posterior distribution of σ_d is peaked around 1 Å, reflecting an estimated error in the distance restraints typical of NMR-based structural refinements (Fig. S2b). The posterior distribution of σ_J is peaked around 5.0, indicating larger experimental uncertainty for the *J*-coupling constants, which is reasonable given the nonlinear relation between dihedral angles and coupling constants that results from the Karplus relations used (Fig. S2c) The posterior distribution of the scaling constant γ' is peaked near $\gamma' = 1$, validating our choice of 3.8 Å for restraining distances according to the observed NOEs (Fig. S2d). Overall, these results are highly consistent with the results of previous calculations performed for cineromycin B (*O*-desmethyl albocycline), a highly similar macrolide.[17]

The ten states with the highest estimated populations can be divided into two main groups, based on their structural similarity to the two isoforms seen in the crystal structure of albocycline[27] (Fig. S3). Conformational states similar to crystal isoform 1 (xtal 1) include states 38, 39, 37, 65, 91 and 59 (conformer A, 34.5% total population), while states 46, 85, 92 and 80 (conformer B, 50.4% total population) are most similar to crystal isoform 2 (xtal 2). This roughly equal distribution of conformational populations is in contrast with the BICePs predictions for the related macrolide cineromycin B (*O*-desmethyl albocycline), which is predicted to populate conformations similar to crystal isoform 1 at ~80%.

2.1.3. Docking calculations of albocycline to MurA enzyme receptor structures and molecular simulation

All-atom simulations were run using Gromacs 4.6.5[20] on the Folding@home distributed computing platform.[28] The initial conformation of *apo*-MurA was prepared by removing all the substrate, water molecules and ions in the crystal structure (PDB: 1UAE). The Amber ff99sb-ildn-nmr force field[29] was used with the TIP3P water model. The system was constructed as a periodic cubic box solvated with 22,776 explicit water molecules and counterions at 0.1 M NaCl. Stochastic (Langevin) dynamics was performed using a time step of 2 fs. Electrostatic energies and forces were computed using the particle-mesh Ewald (PME) method with a 0.12 nm grid spacing and 0.9 nm cut-off. The system was first equilibrated at 300 K and 1 atm in the isothermal-isobaric (NPT) ensemble with Berendsen pressure-coupling. Production runs were performed in the canonical (NVT) ensemble at 300 K coupled to a Berendsen thermostat, in a box of 760.01 nm^3, to obtain 315 μs of aggregate trajectory data.

2.1.4. Markov State Model (MSM) construction

The MSMBuilder3[24] and MDTraj[30] software packages were used in all data analysis and model construction. A total of 63 C_α and C_β atoms were selected from residues in the MurA binding pocket and 1953 pairwise distances were calculated between them. Time-structure based independent component analysis[31,32] (tICA) was performed using a lag time of 5 ns to project the pairwise distance data to a low-dimensional subspace capturing the slowest conformational motions, suitable for constructing Markov State Models via conformational clustering using a *k*-means algorithm. The generalized matrix Rayleigh quotient (GMRQ) method[33] was used to find other optimal MSM model hyper-parameters. The final (optimal) MSM model was constructed using 10 tICA components, 5 ns MSM lag time and 100 MSM microstates, with the choice of lag time validated by implied timescale plots (Fig. S4).

Projection of the simulation trajectory data onto the first two tICA components shows three main conformational basins sampled by *pseudo-apo* MurA (*E. coli*), which we characterize as a closed-form region (top left), half-open-form region (bottom right) and open-form region (top right) (Fig. 2). Conformational clustering via the *k*-means algorithm was used to identify 100 microstates, which mainly distribute across these three basins. To sufficiently sample receptor structures for computational docking and homology model construction, we drew five

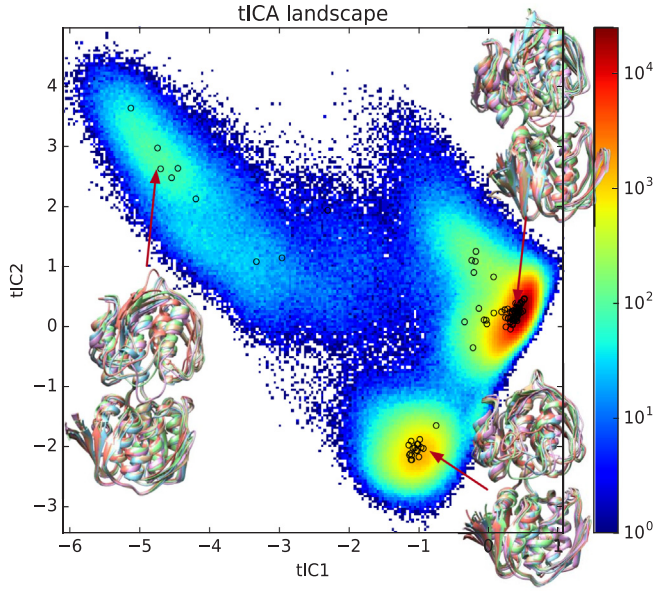

Fig. 2. Projection of the simulation trajectory data onto the first two tICA components shows three main conformational basins sampled by *pseudo-apo* MurA (*E. coli*): a closed-form region (top left), half-open-form region (bottom right) and open-form region (top right). Black circles denote the 100 microstate centers obtained by *k*-means conformational clustering.

random structures from each of the 100 microstates.

2.1.5. Homology model construction

Modeller v9.16 was used to construct *S. aureus* MurA and MurZ homology models[34] using the specific sequences of bacterial strains used in the experimental studies. Five structures randomly drawn from each of the 100 microstates of the MSM were used to generate 500 *E. coli* MurA structures as templates. From these, 500 *S. aureus* MurA and MurZ homology models were built using the sequences and the 500 *E. coli* MurA templates respectively.

2.1.6. Computational docking with DOCK6

Computational docking was performed using UCSF DOCK 6.7.[35] The *E. coli* MurA crystal structure was downloaded from the Protein Data Bank (PDB:1UAE) and processed using the UCSF Chimera *dockprep* tool.[36] Molecular topologies for UDP-GlcNAc and albocycline were constructed based on their crystal conformations, with partial charges assigned using the AM1-BCC method[23] implemented in AmberTools *antechamber*.[37] All 1500 Mur enzyme receptor structures were converted to DOCK-compatible MOL2 files. Grids were computed for each of the receptors at 0.3 Å resolution. Because of its molecular flexibility, UDP-GlcNAc was docked to the *E. coli* MurA structures using an anchor-and-grow algorithm; the two albocycline isoforms were docked rigidly to all the receptors.

Computational docking resulted in a diffuse ensemble of lowest-energy docked poses to each of the 1500 receptor structures. To classify poses into specific binding regions, we used principal component analysis (PCA) to cluster the poses into four groups based on protein-ligand contact distances. For all protein residues within 8 Å (closest heavy-atom) of the native ligands (fosfomycin and UDP-GlcNAc), pairwise atom distances between the residues' C_α atoms and all heavy atoms in albocycline were used as inputs to PCA, which was performed separately for each enzyme. The largest 6 principal components were used for *k*-means clustering into four groups, which were found to be well-separated spatially in the MurA active site, and well-separated in principal component space (Fig. S5).

2.2. Experimental methods

2.2.1. Bacterial strains and culture conditions

E. coli DH5α and BL21 (DE3) strains were from the Grimes' laboratory stock. The well characterized methicillin-sensitive *S. aureus* (MSSA) strain UAMS-1 was provided by Dr. M. Smeltzer (University of Arkansas), whereas the MRSA strain LAC-JE2 and vancomycin-intermediate *S. aureus* (VISA) strain Mu50 were obtained from Dr. P. Fey (University of Nebraska). Vancomycin-resistant strains, VRSA1 and VRSA10, were obtained as clinical isolates from the University of Nebraska Clinical Microbiology Laboratory. Cells were grown in liquid or solid Mueller-Hinton medium. *S. maizeus* was obtained from United States Department of Agriculture (USDA) and cultured with Bennett's medium (ATCC Medium #174) or Yeast Extract-Malt Extract agar. *E. coli* RFM 795 was purchased from the Coli Genetic Stock Center from Yale University (CGSC#: 14179).

2.2.2. Isolation of albocycline from S. maizeus cell culture

S. maizeus cells were grown and spored on Yeast Extract-Malt Extract agar. Cell spores were inoculated into a small amount of Bennett's medium (around 10 mL medium in 25 mm diameter culture tube) and then incubated on a rotary shaker at 28 °C, 200 rpm for 48 to 72 h. This cell culture was added into a 4 L flask containing 1 L of Bennett's medium as production medium. The production flask was incubated at 28 °C, 200 rpm for 4–5 days. After incubation, an equal amount of ethyl acetate (1 L) was used to extract albocycline. Ethyl acetate was added into the flask and mixed with the cell culture by shaking vigorously. Upon settling, the upper organic layer containing albocycline was transferred into a round-bottomed flask and concentrated by rotary evaporation. Albocycline was further purified by silica gel flash column chromatography. The production of albocycline can be analyzed in a TLC system (ethyl acetate: hexanes, 30%: 70%, staining with 10% sulfuric acid), retention factor (R_f) is 0.3. In this study, 30–40 mg of pure albocycline can be isolated from 1 L of *S. maizeus* cell culture. Spectral data (^{1}H and ^{13}C NMR), optical rotation, and R_f values were in full agreement with those reported by Tanner and Okuda.[5,8]

2.2.3. Minimum Inhibitory Concentration (MIC) study

MIC measures of albocycline against *S. aureus*, MSSA (UAMS-1), MRSA (LAC-JE2), VISA (Mu50), VRSA1, VRSA10 and *E. coli* RFM 795 were determined using standard broth microdilution.[38] MIC testing was performed by growing bacteria overnight in Mueller Hinton (MH) 37 °C in a rotary shaker. The bacterial suspension was then diluted (1:100) in fresh media and grown to mid-exponential phase. Ten microliters of cells ($\sim 3 \times 10^5$ Colony Forming Units) were added to individual wells of a 96-well round-bottom plate containing 88 μL of MH and 2 μL of test compound (ranging from 0 to 256 μg/mL). Mixtures were incubated at 37 °C for 16 h, and the MIC was defined as the lowest concentration of albocycline that inhibited bacterial growth as judged by the unaided human eye.

2.2.4. Protein expression and purification

Plasmid pGEX-6P-1,[39] which contains a glutathione *S*-transferase (GST) affinity tag gene, was used in protein expression and purification. *E. coli murA* and *S. aureus murA* and *murZ* genes were PCR amplified from *E. coli* or *S. aureus* genomic DNA. The following conditions were used for the PCR amplification: 95 °C as denaturation temperature for 30 s, 58 °C as annealing temperature for 30 s and 72 °C as elongation temperature for 2 min to amplify the product DNA. *E. coli murA*, and *S. aureus murA* genes were inserted into pGEX-6P-1 vector with 5′ *Eco*RI and 3′ *Xho*I sites to generate pGEX-EcMurA and pGEX-SaMurA plasmids (primer sets are EcMurA-For/EcMurA-Rev, and SaMurA-For/SaMurA-Rev, respectively). *S. aureus murZ* genes were inserted into pGEX-6P-1 vector with 5′ *Bam*HI and 3′ *Xho*I sites to generate pGEX-SaMurZ plasmids (primers are SaMurZ-For/SaMurZ-Rev). All inserted genes

were confirmed by sequencing with plasmid sequencing primers (for pGEX-6P-1 vector, using primer set 5GEX/3GEX). A complete list of primer sequences used in this study is shown in Table S5.

Reconstructed pGEX expression plasmids were transformed into BL21(DE3) competent cells. After transformation, a 10 mL overnight BL21 cell culture was inoculated into 1 L fresh LB medium supplemented with 100 μg/mL carbenicillin antibiotic and incubated until OD_{600nm} reached 0.6. The expression of GST-tagged proteins was induced with 1 mM isopropyl-1-thio-β-d-galactoside (IPTG) at 18 °C for 20 h. Induced cells were harvested by centrifugation (5,000 rpm, 30 min) and resuspended in 20 mL GST lysis buffer [150 mM NaCl, 50 mM Tris, 1 mM dithiothreitol (DTT), pH 7.0, containing 1 protease inhibitor cocktail tablet from Roche]. Cells were disrupted by two passes through a French Press at 10,000 psi and centrifuged at 15,000 rpm for 2 × 15 min to remove the cell debris. The supernatant was loaded onto a protein purification column with Glutathione Sepharose 4 Fastflow beads (GE Healthcare) and incubated at 4 °C for 1 h. The flow through was released and column was washed five times with 20 mL GST wash buffer (500 mM NaCl, 50 mM Tris, 1 mM DTT, 1 mM EDTA, pH 7.0). After the washes, 10 mL GST elution buffer (150 mM NaCl, 50 mM Tris, 1 mM DTT, and 1 mM EDTA, pH 7.0) was added with an appropriate amount of PreScission Protease. The column was incubated at 4 °C overnight and then purified protein was collected. For long-term storage at −20 °C, glycerol (20% final concentration) was added into the protein solution.

2.2.5. Enzymatic reaction conditions

Activity and promiscuity of purified enzymes were studied in the enzymatic reactions. Conditions for each enzymatic reaction are as follows:

MurA/MurZ: To 50 mM Tris, 2 mM KCl buffer (pH 7.5), 200 μM of UDP-GlcNAc (from Sigma-Aldrich), 400 μM PEP, was added 1.0 μg purified MurA/MurZ enzyme per 100 μL reaction sample The reaction was incubated at room temperature for 3 h. Reactions were analyzed with HPLC analysis, as described below.

For inhibition studies, all enzymatic reactions were performed in triplicate at room temperature (25 °C) in reaction buffer containing 50 mM Tris, 2 mM KCl. All reactions were preincubated with 350 nM purified *S. aureus* MurA enzyme, 300 μM phosphoenolpyruvate (PEP) and increasing concentrations of albocycline (0, 250, 500, 750, 1000, 1500, 2000, 3000, 5000 μM) for 10 min. 200 μM UDP-GlcNAc was added after 10 min to start the reaction.

After 3 h, the 100 μL reactions were quenched with an equal volume of 400 mM KOH. 100 μL were taken from the quenched reactions and spun at 15,000 rpm for 25 min in 5000 MWCO Spin-X UF concentrators (Corning, Sigma Aldrich). HPLC separations were performed on an Agilent HPLC using a MonoQ 5/50 GL anion exchange column (GE Healthcare). Separation was performed with a 50 μL injection volume at a flow rate of 0.600 mL/min with the following buffer gradient: 2 min 20 mM ammonium bicarbonate (pH 8.0), 8 min gradient from 20 mM to 500 mM ammonium bicarbonate, 5 min 500 mM ammonium bicarbonate, 5 min 20 mM ammonium bicarbonate. Absorbance was measured at 254 nm. The area under the peaks corresponding to UDP-GlcNAc and EP-UDP-GlcNAc were integrated using the Agilent ChemStation software. The identity of the UDP-GlcNAc and EP-UDP-GlcNAc HPLC traces was confirmed with high-resolution mass spectra (HRMS) ESI run in negative mode on a Thermo Q-Exactive Orbitrap Mass spectrometer (University of Delaware Mass Spectrometry facility). The IC_{50} value was calculated from percent inhibition of MurA fitted using a dose response non-linear regression curve fit in GraphPad Prism 6.

For preincubation studies, *S. aureus* MurA enzyme was pre-incubated with albocycline and UDP-GlcNAc or PEP to study the inhibition mechanism. 1.0 μg purified MurA enzyme was pre-incubated with 650 μM albocycline and 400 μM UDP-GlcNAc or 400 μM PEP on ice for 10 min. 600 μM PEP or UDP-GlcNAc was added to start the reaction. Each pre-incubation condition was prepared in triple replicates. All reactions were incubated at room temperature for 3 h.

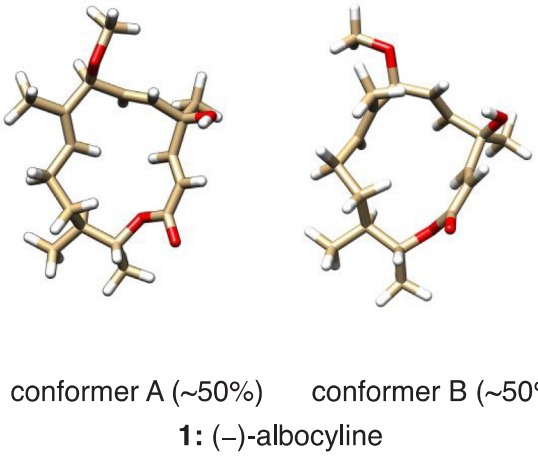

Fig. 3. Albocycline conformers in solution are a mixture of roughly equal populations of conformers A and B (calculated by BICePs and confirmed by ^{1}H NMR).

3. Results and discussion

3.1. Computational modeling

Conformational populations of albocycline (**1**) in solution were calculated via the BICePs algorithm,[17] from measured NOEs and *J*-coupling constants, combined with QM/REMD calculations. The results suggest roughly equal populations of two main conformations, corresponding closely to the two isoforms seen in the X-ray crystal structure of albocycline (Fig. 3),[27] which we will call conformer A and B.

To investigate possible mechanisms of inhibition and test the hypothesis that **1** targets MurA, computational docking studies of albocycline were performed for three Mur enzymes: *S. aureus* MurA, *E. coli* MurA, and *S. aureus* MurZ. Under normal growth conditions, MurA is preferentially expressed compared to MurZ.[40] The substrate-bound crystal structure of *E. coli* MurA in complex with inhibitor fosfomycin (PDB: 1UAE) was used as the basis for homology models of the other variants.

Available MurA crystal structures show great conformational variability in the two lobes defining the active site, as well as the flexible loop regions, which must open and close to allow access to substrate and participation of the catalytic Cys115 residue.[41,42] To prevent bias from the use of any one particular crystal conformation, a molecular simulation-based approach to generating ensembles of receptor structures was pursued. Large-scale molecular dynamics (MD) simulations of *E. coli* MurA were performed on the Folding@home distributed computing network, starting from a *pseudo-holo* structure (PDB:1UAE with UDP-GlcNAc and fosfomycin removed), for an aggregate simulation time of 315 μs. Recent studies using MD-derived receptor ensembles have been shown to improve virtual screening predictions from both known structures and homology models.[43–46] Clustering of the resulting trajectory data was used to construct a Markov State Model of conformational dynamics, from which 500 receptor structures spanning *apo*- to *holo*-like conformations were extracted (Fig. 2), and subsequently used for homology model construction and computational docking studies.

Using each of the MD-derived *E. coli* MurA receptor structures as templates, *S. aureus* MurA and MurZ structures were then built using MODELLER 9.16. DOCK 6.7 was used to perform computational docking of the two albocycline crystal isoforms to the complete ensemble of 1500 receptor structures. While the results of these docking studies are purely prospective, several checks were done to validate their accurate use. First, we verified that the docking algorithm could

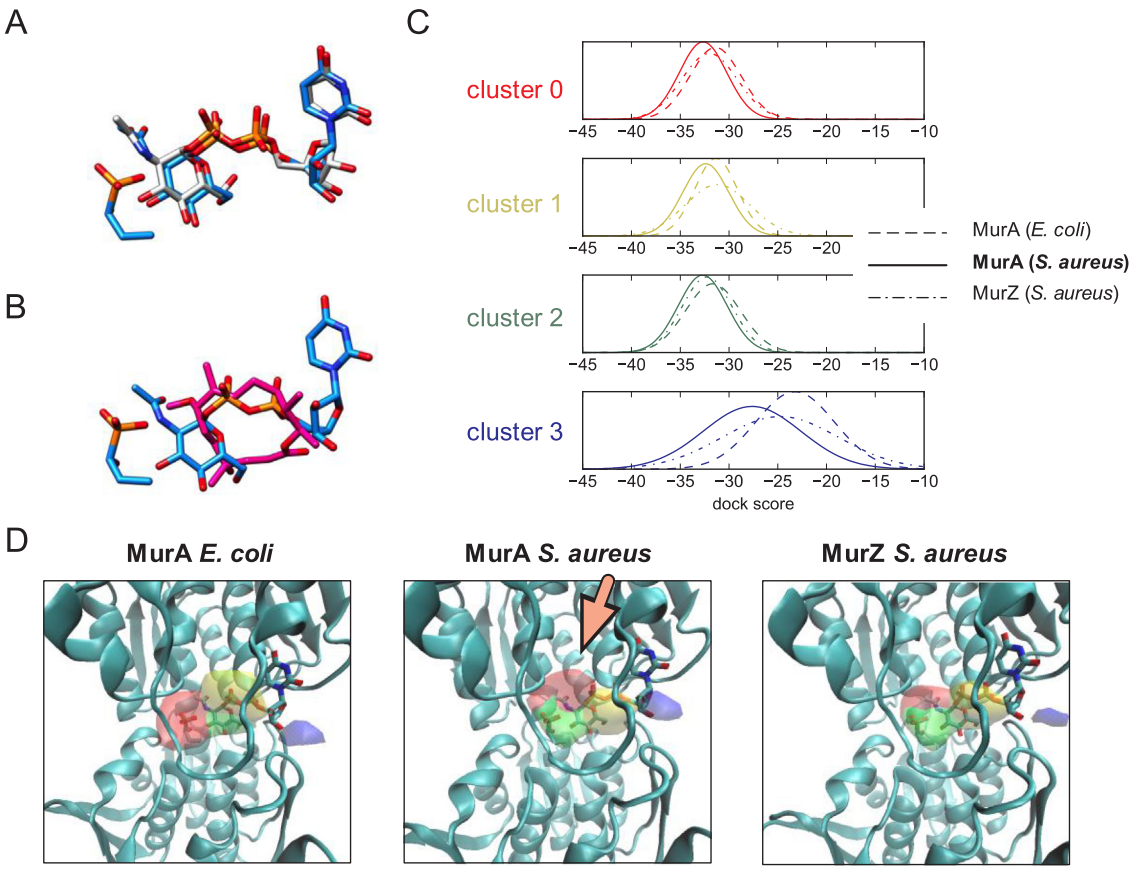

Fig. 4. (A) DOCK 6.7 correctly predicts the pose of UDP-GlcNAc substrate upon re-docking into the MurA (*E. coli*) crystal structure (PDB: 1UAE), to within 1.4 Å rmsd of heavy-atom positions. The crystal poses of fosfomycin and UDP-GlcNAc are shown in blue, and the lowest-energy re-docked pose of UDP-GlcNAc is shown in gray. (B) The lowest-energy docked pose of albocycline (conformer A, magenta) to the Mur A (*E. coli*) crystal structure overlaps with molecular volume available in the UDP-GlcNAc (blue) binding site. (C) Distributions of dock scores for conformational clusters of bound poses, shown here as simplified Gaussians with the same mean and standard deviation to aid the viewer. (D) Average locations of clustered poses (shown as red, yellow, green and blue is surfaces) display notably deeper bound poses for MurA (*S. aureus*, red arrow).

correctly dock UDP-GlcNAc into the original *holo* MurA structure with the substrate removed, to an accuracy of 1.4 Å rmsd in heavy-atom positions (Fig. 4A). Next, we verified that in the absence of substrate, there is sufficient molecular volume to computationally dock albocycline into this structure, with the lowest-energy pose occupying the UDP-GlcNAc binding site (Fig. 4B). Similar results were obtained for *S. aureus* MurA and MurZ receptors built from the *E. coli* MurA crystal structure template.

Next, we clustered the collection of 500 lowest-energy docked poses for each enzyme into four conformational states after projection to principal components derived from protein-ligand contact distances (Fig. S5). While these four states each comprise diffuse collections of bound poses, their locations and average docking scores reveal key differences in how albocycline may bind the three Mur enzymes. Across all four conformational states, average docking scores were consistently lower in energy for albocycline docked to MurA (*S. aureus*) versus MurA (*E. coli*) and MurZ (*S. aureus*), with two-sample *t*-tests verifying the statistical significance of these results (Fig. 4C, Table S4).

One particular state (red isosurface, Fig. 4D) shows the most statistically significant decrease in the average dock score for MurA (*S. aureus*) versus MurA (*E. coli*) (*t*-test *p*-value of 8.9×10^{-13}, Table S3), and docked poses that are visibly deeper in the interior of MurA, towards residue 95. There are only 13 amino acids in the binding site (≤5 Å away from bound ligands) that differ across the three enzymes (Fig. 5).[40]

Whereas MurA (*E. coli*) and MurZ (*S. aureus*) have tryptophan (W) and tyrosine (Y), respectively, at residue 95, MurA (*S. aureus*) has

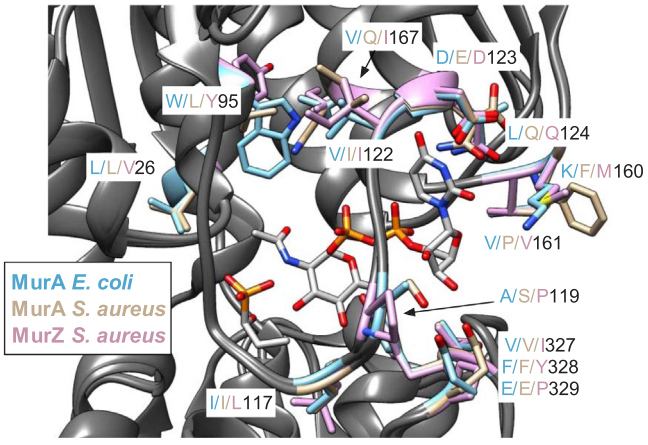

Fig. 5. Sequence variation of residues near the substrate binding site for MurA (*E. coli*, blue), MurA (*S. aureus*, tan) and MurZ (*S. aureus*, lavender). Side chains are shown for all non-conserved residues less than 5 Å from the native bound ligands fosfomycin (gray, left) and UDP-GlcNAc (gray, right) in the MurA (*E. coli*) crystal structure (PDB: 1UAE).

leucine (L), which may provide more volume for albocycline to bind more deeply. We also find a large shift (approximately 2.8 dock score units) in the average MurA (*S. aureus*) dock energy scores for binding poses outside the binding site near the location of the native UDP uridine (blue isosurface, Fig. 4D); however, the average dock scores for

this cluster are higher than the others (Table S4), with only a small minority of lowest-energy poses found in this cluster (Fig. S7). Thus, we suspect the sequence variation at W/L/Y95 is mainly responsible for the selectivity and affinity of binding of albocycline to MurA (*S. aureus*). This hypothesis could be tested in future work using mutational analysis; it is not pursued here for reasons discussed below.

We additionally analyzed the docking results to see if any binding preference was predicted for albocycline conformer A versus B. Average dock scores for all Mur enzyme sequences are slightly lower for conformer A, but these differences are not statistically significant (Fig. S8, Table S4). We also sought to determine if the docking results depend sensitively on the use of closed-form versus open-form simulated receptor structures, by partitioning the dock scores into closed-form versus open-form groups and performing separate analyses. These results yielded the same predictions of selectivity for *S. aureus* MurA (Fig. S6).

3.2. Biological activity of albocycline

To experimentally test the hypothesis that albocycline targets MurA, we evaluated albocycline in biochemical and MIC (Minimum Inhibitory Concentration) assays with material purified from the producing organism, *Streptomyces maizeus*.[5–7] The antimicrobial activity was measured in three independent assays using dimethyl sulfoxide (DMSO) as vehicle.[47] Albocycline's inhibitory effect against *S. aureus* and *E. coli* was determined by standard broth microdilution. The antibiotic fosfomycin, a known inhibitor of MurA, was used as a positive control in these studies (Table 1).[42]

Notably, albocycline showed appreciable antibiotic activity against *S. aureus*, as previously reported.[5] Curiously, albocycline had previously shown no inhibition of Gram-negative *E. coli*, suggesting albocycline could serve as a narrow-spectrum antibiotic.[10] Given the non-polar macrocyclic structure of albocycline, the outer membrane present in Gram-negative *E. coli* could be naturally conferring resistance to albocycline by creating a permeability barrier. To test whether resistance to albocycline was due membrane impermeability, we used a mutant *E. coli* strain (RFM795) containing an *lptD* gene mutation. LptD (Lipopolysaccharide or LPS-assembly protein) is a key protein in the outer membrane, and deletion or disruption of this gene compromises membrane integrity and permeability.[48] *E. coli* RFM795 cell growth was not inhibited by albocycline (MIC $>$ 256 μg/mL), which suggests that membrane penetration most likely does not affect wild-type *E. coli* resistance (Table 1). Fosfomycin was used as a positive control for *E. coli* RFM795 (MIC = 1 μg/mL).

We also measured the antimicrobial properties of albocycline against a panel of notoriously difficult to treat, clinically isolated, and genetically divergent *S. aureus* strains (Table 1), including VISA, MRSA, and VRSA isolates, using vancomycin as comparator.[38] In each case, albocycline displayed impressive antimicrobial properties expected of a pharmaceutical lead antibiotic candidate. Furthermore, albocycline was not toxic to human cells at a final concentration $\leq$64 μg/mL in colorimetric MTT Cell Proliferation Assays using human HepG2 hepatocellular liver carcinoma cells.[49]

Table 1
MIC (μg/mL) values for albocycline, vancomycin, and fosfomycin against the following bacterial strains: *S. aureus*, *E. coli*, Methicillin-Susceptible (MSSA), Methicillin-Resistant (MRSA), Vancomycin-Intermediate *S. aureus* (VISA) and Vancomycin-Resistant *S. aureus* (VRSA) clinical isolates.

Strain	Albocycline	Vancomycin	Fosfomycin
S. aureus (ATCC 25923)	1	Not tested	32
E. coli (RFM 795)	$>$ 256	Not tested	1
MSSA (UAMS-1)	0.5	1	Not tested
MRSA (LAC-JE2)	2	1	Not tested
VISA (Mu50)	2	4	Not tested
VRSA1	4	$>$ 64	Not tested
VRSA10	1	$>$ 64	Not tested

3.3. Mechanistic studies of inhibition

The IC_{50} concentration of albocycline with *S. aureus* MurA was determined using a previously reported HPLC-based activity assay.[26] Briefly, reactions were set up using purified *S. aureus* MurA, which was preincubated with phosphoenolpyruvate (PEP); UDP-GlcNAc was added with increasing concentrations of albocycline. HPLC separation of UDP-GlcNAc from the MurA product EP-UDP-GlcNAc was then performed (Fig. S9b). We note that when MurA was pre-incubated with albocycline and UDP-GlcNAc, the inhibition effect is less than when compared to the pre-incubation reaction sample of MurA with albocycline and PEP (Fig. S11), supporting the computational data that predicts albocycline to complete with UDP-GlcNAc. The IC_{50} was determined from percent inhibition, which was calculated as a function of relative peak areas of UDP-GlcNAc and EP-UDP-GlcNAc (Fig. 6a).

The IC_{50} for albocycline of *S. aureus* MurA's enzymatic activity was calculated to be 480 μM using a non-linear regression curve fit in GraphPad Prism 6 (Fig. 6b). These data indicate that albocycline is a weak inhibitor of *S. aureus* MurA at high micromolar concentrations. Albocycline (**1**) showed no inhibition of *S. aureus* MurZ or *E. coli* MurA, supporting computational findings wherein **1** preferentially binds to *S. aureus* MurA over *E. coli* MurA. However, the high IC_{50} against *S. aureus* MurA suggests that albocycline affects another biological target, either within PG biosynthesis or another pathway that potentially effects flux of PG building blocks (e.g., nucleotide sugars or d-amino acids).

Due to the weak inhibition of *S. aureus* MurA, we have not yet pursued further mutational studies to test whether the sequence variation at W/L/Y95 is responsible for the selectivity of albocycline across MurA variants. More immediate future work will focus on identifying alternative targets.

4. Conclusion

In this work, the macrolactone natural product albocycline (**1**), originally isolated from *Streptomyces* strains, and previously hypothesized by Tomoda and co-workers to exert its biological activity by inhibiting bacterial cell wall biosynthesis, was confirmed to be a potent antibiotic against methicillin- and vancomycin-resistant *S. aureus*. To test the hypothesis that albocycline targets MurA, joint computational and experimental studies were performed.

Computational studies showed that albocycline exists as two conformations in solution, and computational docking to an ensemble of simulated receptor structures suggested that albocycline preferably docks to *S. aureus* MurA over *S. aureus* MurZ and *E. coli* MurA. We then experimentally cultured and isolated albocycline (Fig. S12) from *S. maizeus,* and found it to weakly inhibit MurA from *S. aureus* with an IC_{50} of 480 μM, but not to inhibit *S. aureus* Mur Z (a MurA homolog) or *E. coli* MurA. These results agree well with our computational studies, suggesting that large-scale simulation-based methods for generating receptor structure ensembles[45] can be a promising approach to gain insight to into inhibitor specificity, correctly ranking affinity differences among quite modest inhibitors, and doing so in the absence of crystal structures for all variants of interest.

Although the biochemical and computational studies demonstrate albocycline inhibits MurA, it does so very weakly. Tomoda's reported IC_{50} of albocycline in the [^{3}H]GlcNAc uptake assay (34.5 μg/mL or 112 μM) when compared to its MIC (0.5–1.0 μg/mL or 1.62–3.25 μM) suggests either weak inhibition of MurA is sufficient to destroy the peptidoglycan regulation or there are alternate mechanisms of action (*vide supra*). Recently, Rubin and co-workers demonstrated that MurA from mycobacteria functions as a complex with a regulatory protein that requires a kinase to be activated.[50] It is conceivable that MurA from *S. aureus* functions in a similar manner, which would explain the

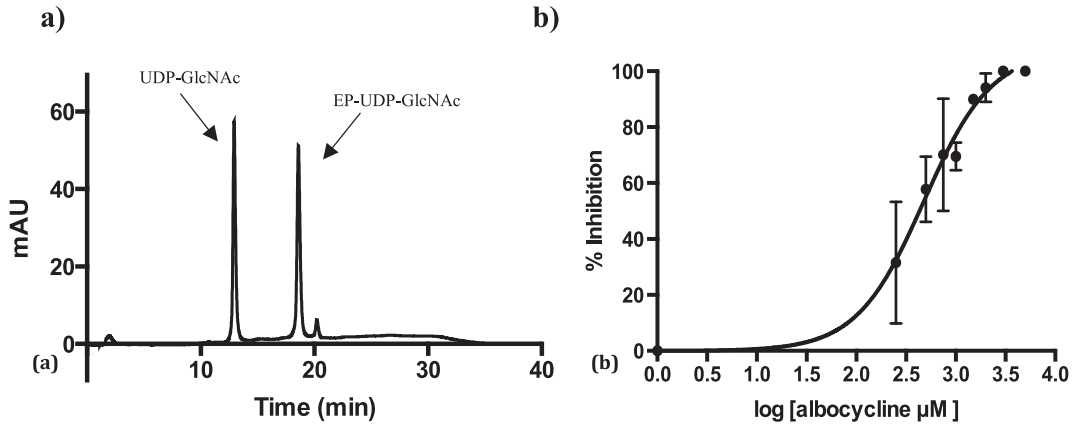

Fig. 6. HPLC-based IC_{50} study of albocycline against *S. aureus* MurA. (a) HPLC trace of the MurA reaction in the presence 250 μM albocycline showing the separation of UDP-GlcNAc and EP-UDP-GlcNAc. (b) IC_{50} data for albocycline and *S. aureus* MurA. Data were fitted using a non-linear regression curve fit in Graph Pad Prism 6.

disparity between albocycline's inhibition effect in the biochemical and MIC assays due to the absence of a cognate regulatory protein in the former.

To evaluate alternative mechanisms of inhibition, we are currently pursuing several strategies to screen for alternative targets. One strategy is to prepare chemical probes of albocycline to screen for alternative targets.[51] Guided by molecular modeling and enabled by access to material, we will prepare analogs via total and semi-synthesis to improve biological activity and physicochemical properties. Another strategy is to perform whole-genome sequencing for albocycline-resistant mutants of *S. aureus*. These results will be reported in due course.

Acknowledgements

The NSF (CHE-1362461 and CHE-1665145) and Temple University supported this research. G.Z., Y.G. and V.V. were supported by NSF MCB-1412508 and through major research instrumentation grant number CNS-09-58854. Support for the NMR facility at Temple University by a CURE grant from the Pennsylvania Department of Health is gratefully acknowledged. CLG is a Pew Biomedical Scholar and thanks the foundation for financial support. Instrumentation support at the University of Delaware was supported by National Institute of General Medical Sciences (NIGMS) through P20GM104316.

A. Supplementary data

Supplementary data associated with this article can be found, in the online version, at http://dx.doi.org/10.1016/j.bmc.2018.05.017.

References

1. Klevens RM, Morrison MA, Nadle J, et al. *JAMA.* 2007;298:1763.
2. Boucher HW, Talbot GH, Bradley JS, et al. *Clin Infect Dis.* 2009;48:1.
3. Sievert DM, Rudrik JT, Patel JB, McDonald LC, Wilkins MJ, Hageman JC. *Clin Infect Dis.* 2008;46:668.
4. Purrello SM, Garau J, Giamarellos E, et al. *Glob Antimicrob Resist.* 2016;7:178.
5. Nagahama N, Suzuki M, Awataguc S, Okuda T. *J Antibiot.* 1967;20:261.
6. Furusaki A, Matsumoto T, Harada K, et al. *Bull Chem Soc Jpn.* 1983;56:3042.
7. Thomas RC, Chidester CG. *J Antibiot.* 1982;35:1658.
8. Tanner D, Somfai P. *Tetrahedron.* 1987;43:4395.
9. Chatare VK, Andrade RB. *Angew Chem Int Ed.* 2017;56:5909.
10. Koyama N, Yotsumoto M, Onaka H, Tomoda H. *J Antibiot.* 2013;66:303.
11. Wilson DN. *Crit Rev Biochem Mol Biol.* 2009;44:393.
12. Brown ED, Vivas EI, Walsh CT, Kolter R. *J Bacteriol.* 1995;177:4194.
13. Slechta L, Cialdella J, Hoeksema H. *J Antibiot.* 1978;31:319.
14. Olesen SH, Ingles DJ, Yang Y, Schonbrunn E. *J Basic Microbiol.* 2014;54:322.
15. Steinbach A, Scheidig AJ, Klein CD. *J Med Chem.* 2008;51:5143.
16. Gersch M, Kreuzer J, Sieber SA. *Nat Prod Rep.* 2012;29:659.
17. Voelz VA, Zhou G. *J Comput Chem.* 2014;35:2215.
18. Ge Y, Voelz VA. *J Phys Chem B.* 2018. http://dx.doi.org/10.1021/acs.jpcb.7b11871.
19. Bergy ME, Hoeksema H, Johnson LRE, Kinch DG. US3651219A; 1972.
20. Pronk S, Pall S, Schulz R, Larsson P, Bjelkmar P, Apostolov R, et al. *Bioinformatics (Oxford, England).* 2013;29:845.
21. Wang J, Wolf RM, Caldwell JW, Kollman PA, Case DA. *J Comput Chem.* 2004;25:1157.
22. Onufriev A, Bashford D, Case DA. *Proteins.* 2004;55:383.
23. Jakalian A, Jack DB, Bayly CI. *J Comput Chem.* 2002;23:1623.
24. Beauchamp KA, Bowman GR, Lane TJ, Maibaum L, Haque IS, Pande VS. *J Chem Theory Comput.* 2011;7:3412.
25. Shirts MR, Chodera JD. *J Chem Phys.* 2008;129:124105.
26. Butterfoss GL, Yoo B, Jaworski JN, et al. *PNAS.* 2012;109:14320.
27. Furusaki A, Matsumoto T, Harada KI, et al. *Bull Chem Soc Jpn.* 1983;56:3042.
28. Shirts M, Pande VS. *Science.* 1903;2000:290.
29. Li D-W, Brüschweiler R. *Angew Chem Int Ed.* 2010;49:6778.
30. McGibbon RT, Beauchamp KA, Harrigan MP, et al. *Biophys J.* 2015;109:1528.
31. Schwantes CR, Pande VS. *J Chem Theory Comput.* 2000;2013:9.
32. Perez-Hernandez G, Paul F, Giorgino T, De Fabritiis G, Noé F. *J Chem Phys.* 2013;139:015102.
33. McGibbon RT, Pande VS. *J Chem Phys.* 2015;142:124105.
34. Webb B, Sali A. *Current protocols in bioinformatics.* John Wiley & Sons Inc; 2014.
35. Allen WJ, Balius TE, Mukherjee S, et al. *J Comput Chem.* 2015;36:1132.
36. Pettersen E, Goddard T, Huang C, et al. *J Comput Chem.* 2004;25:1605.
37. Wang J, Wang W, Kollman PA, Case DA. *J Mol Graph.* 2006;25:247.
38. Reller LB, Weinstein M, Jorgensen JH, Ferraro MJ. *Clin Infect Dis.* 2009;49:1749.
39. Kaelin WG, Krek W, Sellers WR, et al. *Cell.* 1992;70:351.
40. Blake KL, O'Neill AJ, Mengin-Lecreulx D, et al. *Mol Microbiol.* 2009;72:335.
41. Eschenburg S, Schonbrunn E. *Proteins.* 2000;40:290.
42. Skarzynski T, Mistry A, Wonacott A, Hutchinson SE, Kelly VA, Duncan K. *Struct/Fold Des.* 1996;4:1465.
43. Amaro RE, Li WW. *Curr Top Med Chem.* 2010;10:3.
44. Offutt TL, Swift RV, Amaro RE. *J Chem Inf Model.* 1923;2016:56.
45. Mukherjee S, Pantelopulos GA, Voelz VA. *Sci Rep.* 2016;6:31631.
46. Cappel D, Hall ML, Lenselink EB, et al. *J Chem Inf Model.* 2016;56:2388.
47. The concentration of albocycline in DMSO was 50 mg/mL.
48. Sampson BA, Misra R, Benson SA. *Genetics.* 1989;122:491.
49. Mosmann T. *J Immunol Meth.* 1983;65:55.
50. Boutte CC, Baer CE, Papavinasasundaram K, et al. *J eLife.* 2016;5:e14590.
51. Wright MH, Sieber SA. *Nat Prod Rep.* 2016;33:681.